SVU−International Journal of Basic Sciences, VOL. 2, NO. 2, (2025), 48–56

SVU-International Journal of Basic Sciences

Journal homepage: https://svuijbs.journals.ekb.eg/

Research Article:

Mapping structural features and predicting areas of hydrothermal mineral resources using aeromagnetic and remote sensing data

Mona M. Elsoghier[1,*], Mohamed Abedelkareem[1], Mohamed Khalifa[1], Abdelhady M. Akraby [1]

[1]Department of Geology, Faculty of Science, South Valley University, Qena 83523, Egypt.

Article info

Received 7 December 2024
Revised 24 March 2025
Accepted 17 August 2025
Available online 18 August 2025

Keywords:
Aeromagnetic, Landsat-8, ASTER, Hydrothermal Alteration Zones.

Abstract

Aeromagnetic and remote sensing data were used to characterize the lithologic, geologic structures and probable areas of hydrothermal alteration zones in the Marsa Alam area, Eastern Desert of Egypt. The aeromagnetic data was processed and interpreted using several enhancement techniques such as reduction to the pole (RTP), horizontal and vertical derivatives, horizontal gradient magnitude (HGM), tilt angle derivative (TDR), and analytical signal (AS). The results indicated that the NNW, NNE, N-S, NW, NE, E-W, and NE trends are predominant. Furthermore, processing of Landsat-8 Operational Land Imager (OLI) and ASTER remote sensing data allowed mapping of the lithologic characteristics and prediction of the probable areas of hydrothermal alteration zones (HAZs).

1. Introduction

Aeromagnetic data analysis is crucial for geophysical exploration because it allows for a more thorough examination of shallow structures and near-surface sources in high-resolution surveys, in addition to analyzing the regional geological pattern and key structural features (Domzalski, 1966; Elhussein et al., 2024; Minelli et al., 2018). Qualitative analysis of magnetic anomalies provided significant information as the variations in the magnetic body's thickness, folding, topographical relief, and other characteristics can result in these anomalies (Minelli et al., 2018; Kearey & Allison, 1980). Remote sensing data is frequently utilized in geologic, lithologic, and mineral exploration (Sabins,1997; Abdelkareem & El-Baz, 2017; Abdelkareem et al., 2018). This is because of their spatial, radiometric, and spectral resolution variability. Several studies have employed remote sensing data in detecting hydrothermal alteration zones as probable areas of mineral resources and ideal locations for ore deposits (Abdelkareem & El-Baz, 2017; Shi et al., 2020; Sabins, 1999; Poormirzaee & Oskouei, 2010;

Corresponding author:
mona.elmalk13@gmail.com (Mona M. Elsoghier)

DOI: 10.21608/svuijbs.2025.342515.1008

Abdelkareem & Al-Arifi, 2021). Additionally, the geophysical aero-magnetic and spectrometry data provided plausible areas of mineral resources (Gabr et al. 2022; Ghoneim et al., 2021; Maden & Akaryalı, 2015; Shives et al., 1997; Gnojek & Prichystal, 1985; Efimov, 1978).

The integration of disparate geospatial datasets within a Geographic Information System framework facilitates the expedited identification and predictive modeling of prospective mineralized zones. This methodological approach enables the delineation of areas exhibiting optimal potential for mineral resource discovery through the analysis of spatially correlated geological, geophysical, and geochemical variables (Abdelkareem & El-Baz,2017; Abdelkareem& Al-Arifi,2021).

The aim of the present study is to integrate aeromagnetic and remote sensing data for revealing the surface and subsurface geological features and delineate the zones of hydrothermal alteration.

2. Study area:

The study area is located on the Egypt's Red Sea coast, at Marsa Alam area (Fig.1a). It is situated north of the road that links the towns of Marsa Alam and Idfu in the Central Eastern Desert. The area covers approximately 304 km2 and is bounded by Latitudes 25° 8′ N and 25° 30′ N and Longitudes 33° 50′ E and 34° 20′ E. It is a part of the Central Eastern Desert (CED) presented along with the first realistic and applicable succession of rock units (El-Ramly & Akkad, 1960).

The study area is occupied by gneiss domes of the high-grade metamorphic rocks that make up the Meatiq Group of the Eastern Desert (Akaad &Noweir, 1980). The study area built up of Precambrian basement rocks (Fig. 1b) including serpentinites and ultramafic rocks, ophiolitic serpentinite, talc–carbonates, metagabbro-diorite complex, metavolcanics, and metasediments, Older granites, Hammamat Sediments, that intruded by younger granites.

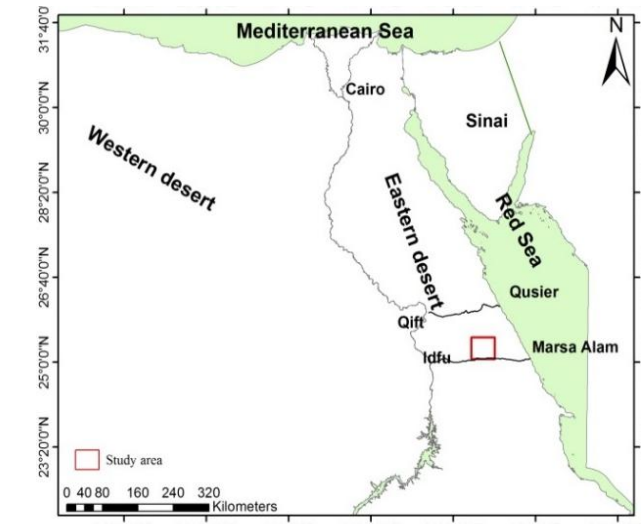

(a)

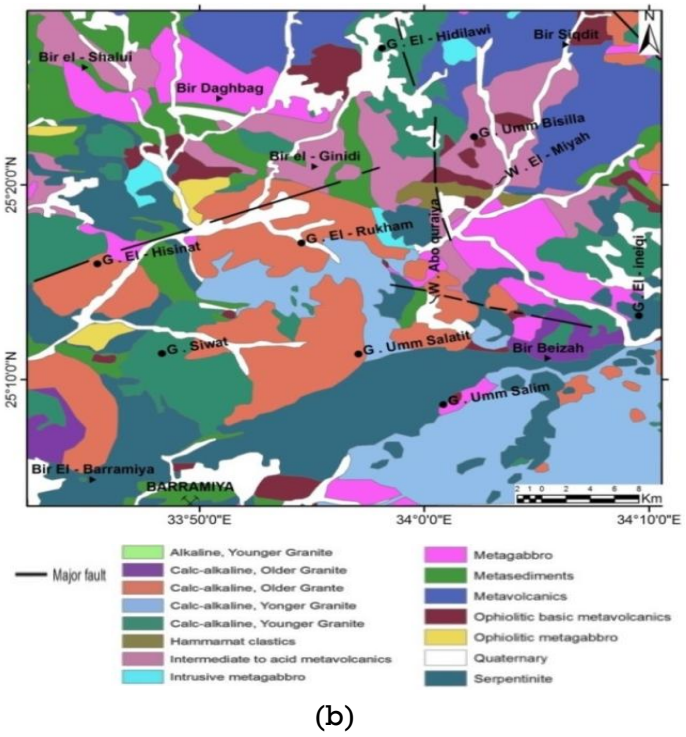

(b)

Figure 1: (a) Location map of the study area marked in red polygon. (b) Geologic map of the study area (EGSMA, 1986).

3. Data and methods:

3.1 Aeromagnetic Data: The Western Geophysical Company of America (Aero Service Division) collected the aeromagnetic data for the study area in 1984 on behalf of the Egyptian General Petroleum Corporation

(EGPC) in collaboration with the Egyptian Geological Survey and Mining Authority (EGSMA, 1986). The aeromagnetic data cover an area of about 304 km². There were two types of flight lines: tie lines flew northwest-southeast at 10-kilometer intervals with an azimuth of 135°/ 315° and traverse flight lines, which were oriented northeast-southwest at a 45°/225° azimuth. Accordingly, the magnetic data undergo several interpretations processing and techniques involving (1) Reduction to the Pole (RTP), (2) regional–residual separation and (3) tilt derivative. These techniques are briefly described below

3.1.1 Reduction to the Pole (RTP): As a result of the well-known effect of inclination and declination on magnetic latitude, which causes anomalies to be shifted from their actual position above causative sources, it can be difficult to comprehend total magnetic intensity (TMI) maps due to the shape and amplitude of magnetic irregularities (Reynolds, 2011). The resulting TMI anomalies are situated at a distance from the source bodies that are causing them. As it is observed at the pole (north magnetic), where the magnetic field is vertical, the effect of the magnetic latitude is reduced when it is removed from the TMI data using a mathematical filter (Baranov & Naudy, 1964). The repositioning of anomalies over their causative sources is referred to as the reduction to the pole (RTP) process.

3.1.2 Regional – Residual Separation: The economically significant anomalies are the residual (local) magnetic anomalies, which are characterized by weaker and more localized anomalies and indicate shallow anomalies. Regional magnetic anomalies are highly significant; in mineral exploration, they are of secondary importance. Low-wavelength anomalies with a deep seat can reveal the deep-seated effects of magnetic sources and identify deep structural elements that influence the research region. Discrete Fourier-transform algorithms can be used to efficiently execute digital filtering operations on digital computers, which are currently utilized for regional-residual separation of anomalies (Dobrin & Savit, 1988).

$$F_2(K_x, K_y) = \begin{cases} 0 & \text{if } K > (2\pi/\lambda s) \\ 1 & \text{elseWhere} \end{cases}$$

$$K = \sqrt{{K_x}^2 + {K_y}^2}$$

3.1.3 Tilt Derivative: The tilt angle map (TAM) is obtained from the first vertical gradient of a magnetic anomaly. The tilt angle's zero contours, used to identify linear features in magnetic data, correspond to the edges of geologic discontinuities. The tilt angle filter was developed by (Verduzco et al., 2004). What is meant by this filter is:

$$\mathrm{TDR} = \tan^{-1}\left(\frac{(\frac{\partial f}{\partial z})}{\sqrt{(\frac{\partial f}{\partial x})^2 + (\frac{\partial f}{\partial y})^2}},\right)$$

where "f" is the magnetic or gravity field and $\partial f/\partial$x, $\partial f/\partial$y, and $\partial f/\partial$z are the first derivatives of the field "f " in the x, y, and z directions. The tilt amplitudes respond to a wide dynamic range of amplitudes for anomalous sources at different depths but are only allowed to reach values between $-\pi/2$ and $\pi/2$. According to (Miller & Singh, 1994), the tilt angle can be utilized to indicate the edges' outline since it yields a zero value over the source edges.

3.2 Remote sensing data: Images from the Advanced Space borne Thermal Emission and Reflection Radiometer (ASTER) and OLI data were collected processed and analyzed using ENVI v.5 and ArcGIS software packages. The wavelengths of electromagnetic radiation in the visible, near infrared, and short-wave infrared (V/NIR/SWIR) are utilized to mapping lithologic characteristics and HAZs (Abdelkareem et al., 2024; Alarifi et al., 2022). The visible and near-infrared bands that an object reflects, along with the intensity of those reflections, provide information about the object's physical properties and chemical makeup. With passive remote sensing, which gauges energy emitted from a natural source (the Sun), visible, NIR, and SWIR waves can be measured.

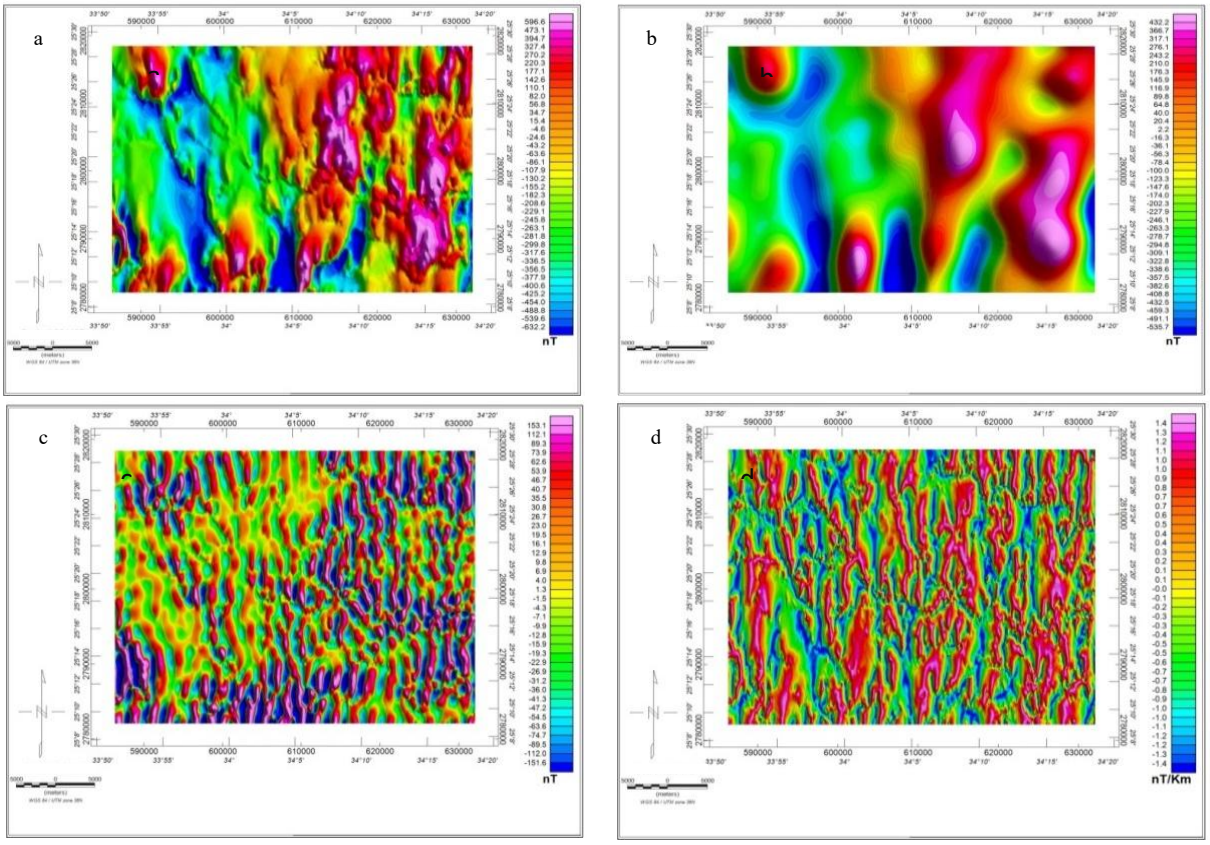

Figure 2: (a) The RTP anomaly map, (b) regional magnetic anomaly map, (c) residual magnetic anomaly map, (d) and the tilt derivative map of the studied area

4. Results and discussions

4.1 Aeromagnetic data

4.1.1. Reduction to the pole (RTP): The earth's surface to deeper levels is represented in the RTP map (Fig. 2a), which illustrates the combined effects of magnetic susceptibilities of various rock types and geological structures. A broad overview of this map shows that magnetic low features predominate in the southwest of the map, while positive magnetic anomaly features dominate the eastern and northern regions. Large positive magnetic anomalies oriented towards the northeast define the eastern region, while elongated positive anomalies oriented towards the north and northwest characterize the northern region. In the eastern and northern regions of the study area, metagabro, metadiorite, serpentines, metavolcanics, and younger granite are associated with a maximum amplitude value of approximately 596.6 nT. Conversely, the lowest amplitude value is roughly – 632.2 nT and is connected to sedimentary rocks in the study area's southwest. The RTP map's magnetic anomalies appear to be structurally regulated in the NE, NW, and N-S directions.

4.1.2 Regional magnetic anomaly map: Smooth, low frequency, homogenous, and high amplitude elongated to rounded closures that form alternating positive and negative magnetic anomaly belts that trend primarily in the NNE, NE, NW, and N-S directions are the general characteristics of the studied area's regional or deep magnetic anomaly map (Fig. 2b). The RTP and regional magnetic maps exhibit a strong correlation in the distribution and trend of both high and low magnetic zones across the studied region, despite their apparent.

4.1.3 Residual magnetic anomaly map: The alternating belts of high-resolution, high-frequency positive and negative magnetic anomalies are depicted in the residual or shallow magnetic anomaly map (Fig. 2c). These belts consist of interconnected elon-

gated to rounded magnetic anomaly closures with varying orientations, frequencies, and amplitudes. The presence of steep gradients and elongated anomalies, as well as the alternation between positive and negative anomalies, suggest the presence of contacts or faults that split the studied area into multiple blocks with varying magnetization contrasts. The residual map revealed that the WNW, NW, NNE, NE, E-W, and N-S directions are the primary structural trends.

4.1.4 Tilt derivative: It used to distinguish between contacts, boundaries, and structures; to sustain localized strong and weak magnetic anomalies. The vertical contact model is affected by anomalous sources whose horizontal location is detected and whose edges expand. The zero contours, which estimate the location of unexpected shifts in source bodies, are examined. The TDR map (Fig. 2d) examinations reveal that the NW, NNE, NE, and N–S directions are the primary trends of anomalies and lineaments in the map.

4. 2 Remote sensing data: Various band ratios were statistically analyzed using OIF (Table 1.) e.g., band ratio composite 6/7, 4/2, and 5/6 (Abrams ratio) (Abrams et al. , 1982), 6/7, 4/2, 4/6 (Sabins ratio) (Sabins 1997), 6/7, 6/5, 4/2 (Chica-Olma ratio) (Chica-Olmo, 2002), 7/5, 5/4, 6/7 (Kufman ratio) (Kaufmann, 1988), 6/7, 6/5, 5 (Ramadan ratio) (Ramadan et al., 2004), and 6/7, 6/2 and 6/5*4/5 (Sultan ratio) (Sultan et al. 1988). The results revealed high OIF (2877.31) of band ratio composite 6/7, 6/2 and 6/5*4/5 (Table 1.; Fig.3).

Using band ratio composite 6/7, 6/2 and 6/5*4/5 (Sultan et al. 1988) allowed distinguishing between the different rock units (Fig. 4). This is because band ratio 6/7 is sensitive to OH-bearing minerals, and 6/2 is sensitive to opaque minerals (like magnetite). Moreover, band ratio 6/5*4/5 can be used to distinguish between mafic and non-mafic rocks based on their sensitivity to Fe-bearing aluminosilicate concentration. The results revealed that serpentinites, granites, metavolcanics, appear in blue, green, and blue, respectively. However, the hydrothermal alteration zones highlighted in white tone. to mostly represent the areas of higher alteration zones in these color composites. Visible lineaments can be seen in the band ratio composite images of 6/7,

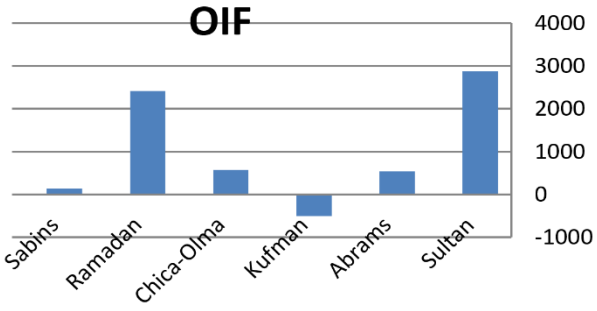

Figure 3: OIF for color composites of band ratios of Sabins, Ramadan, Chica-Olma, Kufman, Abrams, and Sultan.

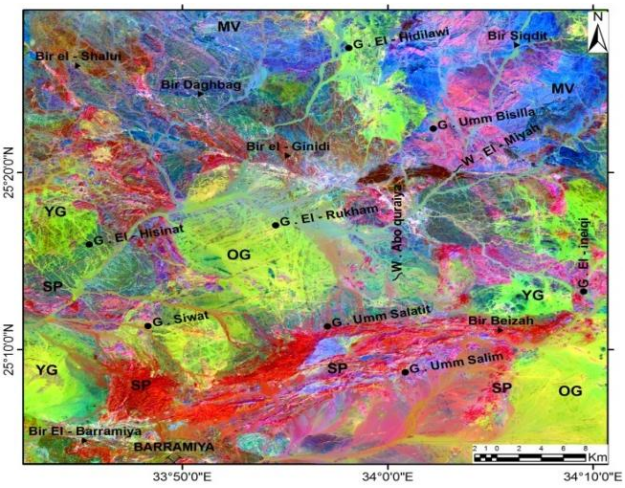

Figure 4: Band ratio composite 6/7, 6/2, 6/5 * 4/5 (Sultan et al. 1988).

Further analysis using ASTER band composites 4, 5, and 6 (Fig. 5) allowed differentiation between mafic (dark tone) and felsic rocks (white tone). Based on that the hydrothermal alteration zone can be highlighted by band 4, this is because the hydrothermal alteration minerals exhibit strong reflection in the spectral region covered by band 4 of the ASTER image and high absorption in bands 5, 6, and 7. Using band ratio 4/2, 4/5, and 5/6 in R, G, and B allowed discriminat-

ing between the mafic rocks in red and the felsic in blue colors (Fig.5b). To differentiate the mineralization zone, mineral indices were employed (Ninomiya, 2004) include OH-bearing altered minerals (OHI), kaolin ite (KLI), and alunite (ALI). In this composite, hydrothermal alteration zones, clearly detected in white tone (Fig. 6). These zones are the potential areas for ore deposits as the hydrothermal fluids circulation has the significant impact on HAZs and mineralization processes.

Table 1. OIF of the selected band ratios

Combination	Sabins	Ramadan	Chica-Olma	Kufman	Abrams	Sultan
Formula	6/7, 4/2, 4/6	6/7, 6/5, 5	6/7, 6/5, 4/2	7/5, 5/4, 6/7	6/7, 4/2, 5/6	6/7, 6/2, 6/5*4/5
OIF	137.18	2410.01	574.68	-503.18	533.54	2877.31

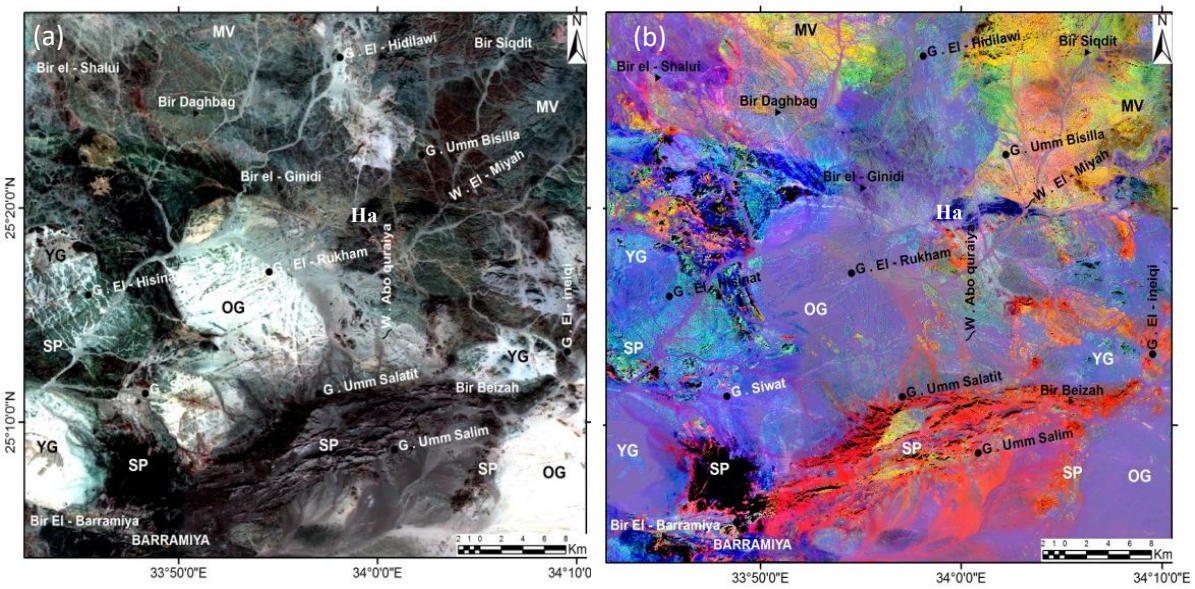

Figure 5: (a) ASTER band composite 4, 5, 6 in R, G, and B; (b) Alteration zone in yellowish red color, band ratio 4/2, 4/5, and 5/6 in R, G, and B.

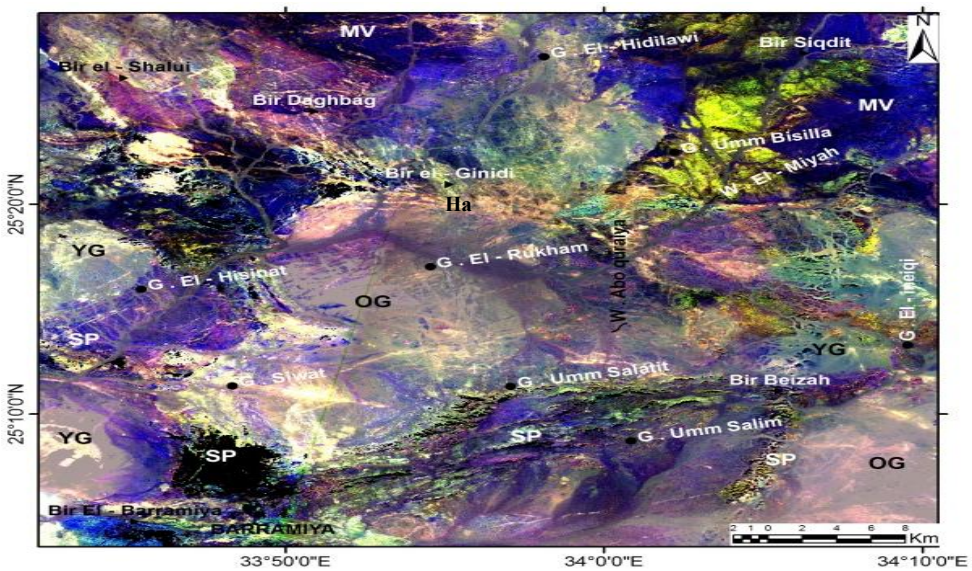

Figure 6: OHI, KLI, and ALI in R, G, and B

5. Conclusions

Integration of aeromagnetic and remote sensing data allowed characterizing the geologic features, lithologic structures, and HAZs at Marsa Alam area, Eastern Desert of Egypt. Several trends such as NNW, NNE, N-S, NW, NE, E-W, and NE are characterized by aeromagnetic data. Processing of Landsat-8 OLI and ASTER data revealed the probable areas of hydrothermal alteration zones (HAZs) and characterizing between the different rock varieties.

Funding Details: No funds have been obtained

Conflict of interest: No conflict of interest is disclosed by the authors.

References

Abdelkareem, M., & Al-Arifi, N. (2021). Synergy of remote sensing data for exploring hydrothermal mineral resources using GIS-based fuzzy logic approach. *Remote Sensing*, *13*(22), 4492.

Abdelkareem, M., & El-Baz, F. (2018). Characterizing hydrothermal alteration zones in Hamama area in the central Eastern Desert of Egypt by remotely sensed data. *Geocarto International*, *33*(12), 1307-1325.

Abdelkareem, M., Abdalla, F., & Yousef, S. (2024). The use of ASTER and landsat remote sensing data for exploring hydrothermal mineral in Arabian-Nubian Shield. *Kuwait Journal of Science*, *51*(3), 100240.

Abdelkareem, M., El-Din, G. M. K., & Osman, I. (2018). An integrated approach for mapping mineral resources in the Eastern Desert of Egypt. *International journal of applied earth observation and geoinformation*, *73*, 682-696.

Abrams, M. J., Brown, D., Lepley, L., & Sadowski, R. (1983). Remote sensing for porphyry copper deposits in southern Arizona. *Economic Geology*, *78*(4), 591-604.

Akaad, M. K., & Noweir, A. M. (1980). Geology and lithostratigraphy of the Arabian Desert orogenic belt of Egypt between latitudes 25◦ 35′ and 26◦ 30′ N. *Evolution and mineralization of the Arabian–Nubian Shield*, Institute of Applied Geology, Jeddah, Bulletin 4, 127–134. Cairo University, pp. 369– 394.

Alarifi, S. S., Abdelkareem, M., Abdalla, F., Abdelsadek, I. S., Gahlan, H., Al-Saleh, A. M., & Alotaibi, M. (2022). Fusion of multispectral remote-sensing data through GIS-based overlay method for revealing potential areas of hydrothermal mineral resources. *Minerals*, *12*(12), 1577.

Baranov, V., & Naudy, H. (1964). Numerical calculation of the formula of reduction to the magnetic pole. *Geophysics*, *29*(1), 67-79.

Chica-Olmo, M., Abarca, F., & Rigol, J. P. (2002). Development of a decision support system based on remote sensing and GIS techniques for gold-rich area identification in SE Spain. *International Journal of Remote Sensing*, *23*(22), 4801-4814.

Dobrin, M. B., & Savit, C. H. (1960). *Introduction to geophysical prospecting* (Vol. 4). New York: McGraw-hill.

Domzalski, W. (1966). Importance of aeromagnetics in evaluation of structural control of mineralization. *Geophysical Prospecting*, *14*(3), 273-291.

Efimov, A.V., (1978). Multiplikativnyj pokazatel dlja vydelenija endogennych rud poaerogamma-spektrometriceskim dannym. Metody rudnoj geofiziki, Leningrad, Naucno-proizvodstvennoje objedinenie geofizika.

EGSMA, (1986). Geology of Wadi As Saqiyah area: Regional geological and

structural map 1:100,000. Internal report No. 64/1999.

Elhussein, M., Barakat, M. K., Alexakis, D. E., Alarifi, N., Mohamed, E. S., Kucher, D. E., ... & Youssef, M. A. (2024). aeromagnetic data analysis for sustainable structural mapping of the Missiakat Al Jukh Area in the central eastern desert: Enhancing resource exploration with minimal environmental impact. *Sustainability*, *16*(20), 8764.

El-Ramly, M. F. (1960). The basement complex in the central Eastern Desert of Egypt between latitudes 24 30 and 25 40 N. *Geological Survey of Egypt*, 33.

Gabr, S. S., Diab, H., Fattah, T. A. A., Sadek, M. F., Khalil, K. I., & Youssef, M. A. (2022). Aeromagnetic and Landsat-8 data interpretation for structural and hydrothermal alteration mapping along the Central and Southern Eastern Desert boundary, Egypt. *The Egyptian Journal of Remote Sensing and Space Science*, *25*(1), 11-20.

Ghoneim, S. M., Abd El Nabi, S. H., Yehia, M. A., & Salem, S. M. (2021). Using air-borne gamma ray spectrometry and remote sensing data for detecting alteration zones around Wadi Saqia area, Central Eastern Desert, Egypt. *Journal of African Earth Sciences*, *178*, 104181.

Gnojek, I., & Přichystal, A. (1985). A new zinc mineralization detected by airborne gamma-ray spectrometry in northern Moravia (Czechoslovakia). *Geoexploration*, *23*(4), 491-502.

Kaufmann, H. (1988). Mineral exploration along the Aqaba—Levent structure by use of Landsat TM data; Concepts, processing and results. International Journal of Remote Sensing, 9(10-11), 1639-1658.

Kearey, P., & Allison, J. R. (1980). A geomagnetic investigation of Carboniferous igneous rocks at Tickenham, County of Avon. *Geological Magazine*, *117*(6), 587-593.

Maden, Nafiz, and Enver Akaryalı. "Gamma ray spectrometry for recognition of hydrothermal alteration zones related to a low sulfidation epithermal gold mineralization (eastern Pontides, NE Türkiye)." *Journal of Applied Geophysics* 122 (2015): 74-85.

Miller, H. G., & Singh, V. (1994). Potential field tilt—a new concept for location of potential field sources. *Journal of applied Geophysics*, *32*(2-3), 213-217.

Minelli, L., Speranza, F., Nicolosi, I., D'Ajello Caracciolo, F., Carluccio, R., Chiappini, S., ... & Chiappini, M. (2018). Aeromagnetic investigation of the central Apennine Seismogenic Zone (Italy): From basins to faults. *Tectonics*, *37*(5), 1435-1453.

Ninomiya, Y. (2004, February). Lithologic mapping with multispectral ASTER TIR and SWIR data. In *Sensors, Systems, and Next-Generation Satellites VII* (Vol. 5234, pp. 180-190). SPIE.

Poormirzaee, R., & Oskouei, M. M. (2010). Use of spectral analysis for detection of alterations in ETM data, Yazd, Iran. *Applied Geomatics*, *2*(4), 147-154.

Ramadan, E., Feng, X. Z., & Cheng, Z. (2004). Satellite remote sensing for urban growth assessment in Shaoxing City, Zhejiang Province. *Journal of Zhejiang University-SCIENCE A*, *5*(9), 1095-1101.

Reynolds, J. M. (2011). An introduction to applied and environmental geophysics (2nd editio). Wiley-Blackwell.

Sabins, F. F. (1999). Remote sensing for mineral exploration. *Ore geology reviews*, *14*(3-4), 157-183.

Sabins, F., (1997): Remote Sensing Principles and Interpretation. Third ed., W.H. Freeman Company, 494.

Shi, X., Al-Arifi, N., Abdelkareem, M., & Abdalla, F. (2020). Application of remote

sensing and GIS techniques for exploring potential areas of hydrothermal mineralization in the central Eastern Desert of Egypt. *Journal of Taibah University for Science*, *14*(1), 1421-1432.

Shives, R. B., Charbonneau, B. W., & Ford, K. L. (2000). The detection of potassic alteration by gamma-ray spectrometry—recognition of alteration related to mineralization. *Geophysics*, *65*(6), 2001-2011.

Sultan, M., Arvidson, R. E., Duncan, I. J., Stern, R. J., & El Kaliouby, B. (1988). Extension of the Najd shear system from Saudi Arabia to the central Eastern Desert of Egypt based on integrated field and Landsat observations. *Tectonics*, *7*(6), 1291-1306.

Verduzco, B., Fairhead, J. D., Green, C. M., & MacKenzie, C. (2004). New insights into magnetic derivatives for structural mapping. *The leading edge*, *23*(2), 116-119.